Influence of the Growth Substrate on the Internal Quantum Efficiency of Algan/Aln Multiple Quantum Wells Governed by Carrier Localization

Gwenolé Jacopin, Christian Frankerl, Nadine Tillner, Matthew John Davies, Georg Rossbach, Christian Brandl, Marc Patrick Hoffmann, Roland Zeisel, Axel Hoffmann, Hans-Jürgen Lugauer

Influence of the growth substrate on the internal quantum efficiency of AlGaN/AlN multiple quantum wells governed by carrier localization

Gwénolé Jacopin,[1,*] Christian Frankerl,[2,3] Nadine Tillner,[2,4] Matthew John Davies,[2] Georg Rossbach,[2] Christian Brandl,[2] Marc Patrick Hoffmann,[2] Roland Zeisel,[2] Axel Hoffmann[3] and Hans-Jürgen Lugauer[2]

1. *Université Grenoble Alpes, CNRS, Grenoble INP, Institut Néel, 38000 Grenoble, France*
2. *OSRAM Opto Semiconductors GmbH, Leibnizstr. 4, 93055 Regensburg, Germany*
3. *Institut für Festkörperphysik, Technische Universität Berlin, Hardenbergstr. 36, 10623 Berlin, Germany*
4. *Institut für Halbleitertechnik, TU Braunschweig, Hans-Sommer-Straße 66, 38106 Braunschweig, Germany*

**E-mail : gwenole.jacopin@neel.cnrs.fr*

ABSTRACT

The influence of the growth substrate on the internal quantum efficiency (IQE) of deep ultraviolet (UV) light emitting diodes is studied. Two nominally identical Al-rich AlGaN/AlN multi-quantum-well (MQW) structures grown by metalorganic vapour phase epitaxy (MOVPE) on different substrates were investigated. The first MQW structure was grown on a native AlN substrate, while the second one was deposited on an AlN template on sapphire. By the combination of atomic force microscopy (AFM), photoluminescence (PL) and cathodoluminescence (CL) spectroscopy, we demonstrate that the dislocation-mediated spiral growth of MQWs on sapphire results in the more efficient localization of carriers. This effect helps to prevent non-radiative carrier recombination at point defects, improving the IQE of the structure.

I. INTRODUCTION

For a large number of applications ranging from water purification and phototherapy to sensing, efficient light sources emitting in the UV spectral range are required.[1] Up to now, the majority of commercially available devices are based on mercury-vapor lamps. However, in 2017 the Minamata convention entered into force, which intends to gradually ban products containing mercury. A promising alternative to mercury-vapor lamps are III-nitride UV light emitting diodes (LEDs). These devices possess a large number of advantages, like they are environmentally friendly, have superior product lifetimes and offer short switch times. However, despite intense research efforts on UV-C LEDs for more than two decades, the external quantum efficiency (EQE) of such devices remains below 20%.[2] Several reasons are generally accepted in literature to explain this relatively low value: (1) Poor doping efficiency due to the high activation energy of dopants in AlGaN layers, (2) poor light extraction efficiency, and most importantly, (3) poor crystal quality, which leads to efficient non-radiative recombination of carriers at threading dislocations and point defects, hence significantly limiting the maximum achievable IQE.[3,4]

In this paper, in order to better understand the impact of dislocations and growth morphology on the growth of AlGaN/AlN MQW structures for use in DUV LED devices, we compare two nominally identical MQW structures grown by MOVPE on different growth substrates. The impact of the growth

substrate on emission properties, light output and IQE is studied by AFM, PL and CL spectroscopy and the crucial role of carrier localization is investigated and discussed in greater detailed.

II. SAMPLE STRUCTURE AND MEASUREMENT METHODS

Two MQW structures were deposited by MOCVD on two different substrates, a native AlN substrate and a sapphire substrate. As illustrated in figure 1(a), Sample A was grown on an AlN native substrate with a threading dislocation density (TDD) of $< 10^4$ cm^{-2}, followed by a 1000 nm thick AlN layer homoepitaxially grown by MOCVD. Conversely, sample B (figure 1(b)) was grown on a single side polished sapphire substrate followed by a 3 µm thick AlN buffer layer resulting in a significantly higher TDD of 2×10^9 cm^{-2}. The MQW structure of both samples is deposited by MOCVD in a N_2/H_2 atmosphere with a constant growth temperature for the wells and barriers of ~ 1025 °C. The V/III ratio of the barriers and wells are ~ 9715 and ~ 3912, respectively. The MQW active region consists of five 1.5 nm thick $Al_{0.45}Ga_{0.55}N$ QWs separated by 4 nm thick AlN barriers. The growth of AlN barriers was intended to improve carrier confinement and to minimize thermal escape.[5,6] Finally, a 50 nm thick AlN capping layer was grown to reduce carrier surface effects such as band banding due to Fermi level pinning.[7] Both samples were deposited under identical growth conditions (V/III ratios, growth temperature, etc.) in the same growth reactor. However, the growth mode of the both samples varies significantly, due to the large difference in TDD, which is discussed in more detail during the result interpretation.

Time-integrated, temperature-dependent PL measurements are conducted using 5th harmonic Nd:YAG laser system ($\lambda = 213$ nm, $\tau = 1$ ns, $f_{rep} = 1$ kHz) and a closed-cycle Helium cryostat and IQE values are determined by comparing the maximum PL efficiency values at both 295 K and 12 K. This approach is commonly labelled "High Temperature/Low Temperature" method (references from above) and believed to work adequately when the excitation is resonant and a "plateau region" of the PL efficiency as a function of excitation power density is observed at low temperatures.[4,6] Time-resolved and time-integrated CL measurements were performed in an FEI Inspect F50 SEM. A Horiba Jobin Yvon ihR550 spectrometer equipped with a Peltier-cooled charge coupled device detector and a 600 grooves/mm diffraction grating was used for spectral analysis. For time-resolved measurements, a combination of a

homemade fast beam-blanker and a fast photodetector has been used. With this configuration, the temporal resolution is estimated to be better than 50 ps.[8] To achieve such a temporal resolution, the acceleration voltage was reduced to 3 kV.[9]

III. RESULTS AND DISCUSSION

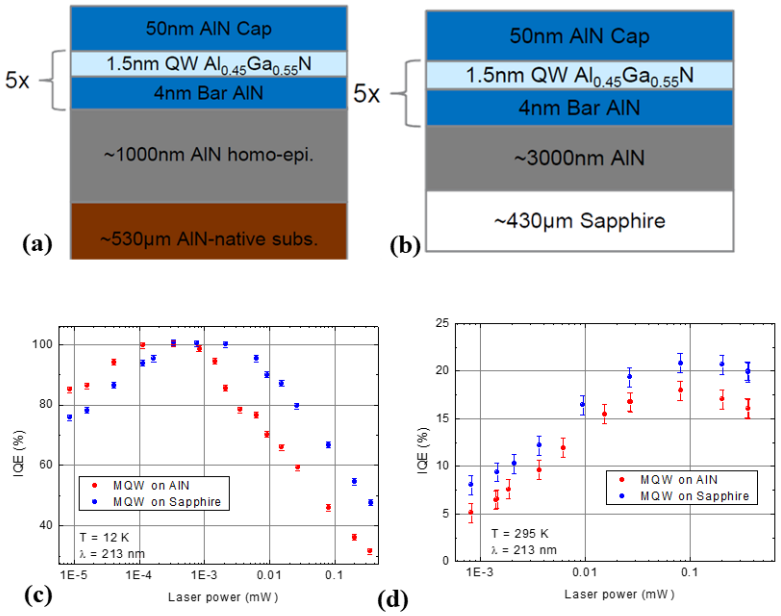

Fig. 1. (a, b) Sketch of the two investigated MQW structures structures grown on an AlN substrate (a) and a sapphire substrate, respectively (b). (c, d) PL IQE as a function of the excitation power density for both samples defined at 12 K (c) and 295 K (d).

First, excitation power density-dependent PL efficiency measurements were performed to estimate the IQE of the two samples both at 12 K and 295 K. As illustrated in figure 1(c), the PL efficiency is constant over a full order of magnitude in both structures at 12 K, indicating an IQE of 100%. As the carrier lifetimes at 12 K of both samples are comparable (see further measurements), the carrier densities injected into the structures is directly proportional to the applied laser power. According to the ABC model,[4,6] the maximum of the PL efficiency curve is obtained at $n=\sqrt{(A/C)}$, where n is the carrier density, A is the Shockley-Read-Hall recombination coefficient and C is the Auger coefficient. Assuming that C is constant, the incorporation of point defects in sample B is found to be substantially larger than in sample A, as the maximum of the PL efficiency curve is obtained at higher excitation power densities. As threading dislocations introduce local strain fields[10], the local formation probability for point defects

might change, providing a possible explanation for the larger point defect density observed in sample B. We then employ the common approach of calculating the ratio of the PL integrated intensity at 300 K in relation to that at 12 K in order to estimate the IQE at room temperature.[4,11,12] Against common beliefs, result shown in figure 1(d) indicates that the IQE of the sample grown on sapphire substrate is slightly higher than the one grown on AlN native substrate, in spite of its much higher TDD. More precisely, we estimate a maximum IQE around ~18% for sample A and ~21% for sample B. This is in sharp contrast to the widely accepted model predicting a beneficial effect of the reduction of the TDD on the resulting IQE.[13] It is also worth noting that the peak IQE is achieved at roughly the same excitation power density for both samples at room temperature despite the significant difference observed at low temperature. As already discussed, the 12 K data suggests that sample B contains a greater density of point defects, indicating that – at room temperature – the sample should also go into droop at higher excitation power densities than sample A. This is, however, not observed and already hints at the presence of an additional effect surpassing the simple ABC rate equation model of carrier recombination.

In order to explain the observed difference in maximum IQE, a strain-mediated mechanisms may be responsible.[14] Hence, to evaluate the strain state of the AlN below the MQW region, high resolution CL spectra of the near band edge (NBE) emission at T = 5 K were acquired for both samples and are depicted in figure 2(a). The donor bound exciton peak ($D^{\circ}X_A$) is observed at 6.037 eV (6.078 eV) in sample A (sample B). The shift in energy observed between the two samples can be ascribed to a difference in the AlN strain state. Assuming a biaxial strain,[15] the residual strain in the AlN template grown on sapphire is estimated to yield approximately 0.09%. Given the large lattice mismatch between AlN and sapphire

(13.3%),[16] the AlN template can be considered as fully relaxed. It is thus expected that strain only plays a minor role in the optical properties of both samples and cannot explain the deviating IQEs.

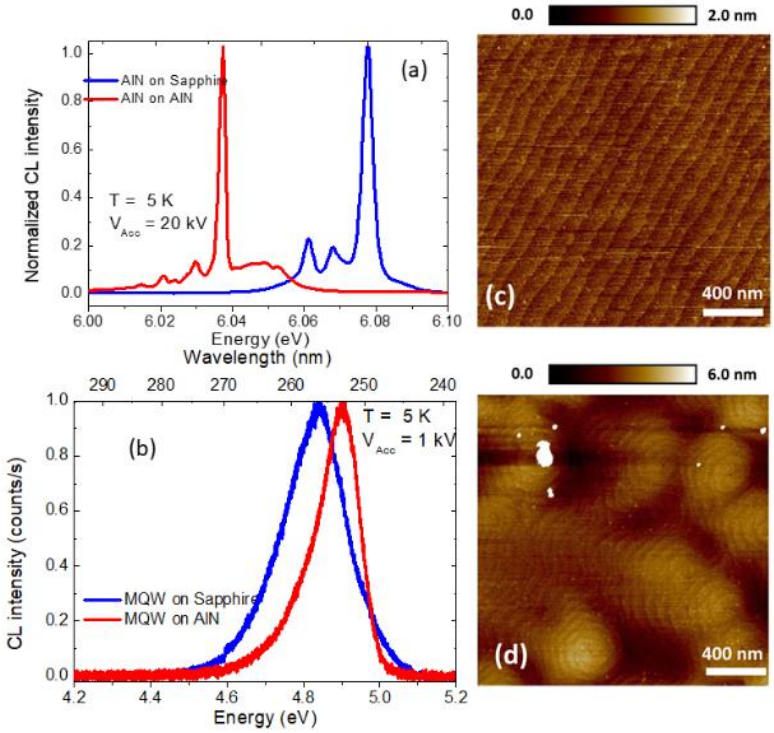

Fig. 2. (a) Corresponding CL NBE emissions at T = 5 K with an acceleration voltage of 20 kV. (b) CL spectra of the MQW region of sample A (red) and sample B (blue) at T = 5 K with an acceleration voltage of 1 kV. (c, d) 2x2 µm^2 AFM images of the two sample structures: MQW on AlN substrate (c), MQW on sapphire substrate (d).

The CL spectra recorded at T = 5 K with an acceleration voltage of 1 kV are displayed in figure 2(b). Both samples show similar peak emission wavelengths between 250 and 260 nm with a noticeable difference in spectral broadening. The full width at half maximum (FWHM) of sample A is 140 meV, while the FWHM of sample B is significantly larger (210 meV). As such, the difference in spectral broadening may indicate different degrees of carrier localization between the two samples.

As shown by Houston Dycus *et al*., the surface morphology during the growth may influence the optical properties of the MQW grown on different substrates.[17] To clarify this point, AFM measurements were performed to assess the surface morphology after growth. AFM images of the samples are shown in figure 2(c) and 2(d). The investigated samples exhibit strongly deviating surface morphologies which suggests different growth modes induced by the high difference in TDD of the Samples A and B. In figure 2(c), the 2 × 2 μm^2 AFM image of the surface of sample A reveals regularly spaced terraces, indicating a low dislocation density as well as step-flow growth.[18] The terrace length is about 60 nm, consistent with the AlN substrate misorientation angle of approximately 0.3°. Conversely, as observed from the AFM image on Sample B shown in figure 2(d), the surface exhibits spirals pinned at dislocations (with c+ component), indicating spiral dominated growth. The dislocation type is either screw or mixed type.[19]

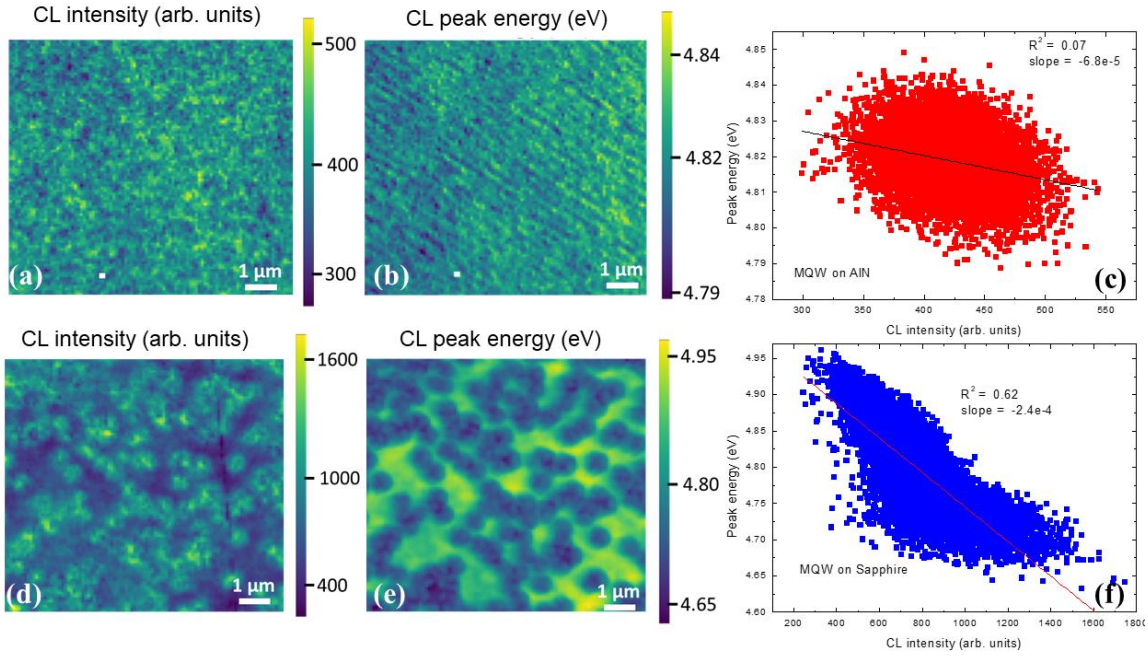

Fig. 3. (a, d) CL intensity of the MQW emission of sample A (a) and sample B (d) at 300 K with an acceleration voltage of 5 kV. (b, e) CL peak energy obtained by Gaussian fitting of the MQW CL emission spectra for sample A (b) and sample B (e). (c, f) Correlation between CL intensity and peak energy for sample A (c) and sample B (f).

To get more insight into the influence of the growth substrate on the IQE of the active region, we performed spatially and spectrally resolved CL spectroscopy on both samples to correlate the surface morphology to the optical properties in the nanoscale region. An acceleration voltage of 5 kV was

applied to efficiently and predominantly excite the MQW region. Room temperature CL spectra were recorded every 100 nm on a square of 10 µm x 10 µm using a Peltier cooled CCD coupled to a spectrometer. Firstly, we observe that sample B is, on average, two times brighter than sample A, consistent with resonant PL measurements. In addition, by fitting the MQW CL emission spectra with a Gaussian profile, the spatial distribution of CL peak energies is acquired. From a CL intensity map performed on sample A (Figure 3(a)), no particular pattern but rapid spatial variation of the CL intensity with no obvious spatial correlation is observed. The CL intensity variation from point to point is characterized by a standard deviation of only 7%, suggesting relatively homogeneous emission. On the contrary, the CL peak energy map displayed in figure 3(b) reveals a regular stripe pattern, equally spaced by around 320 nm. Since this value is more than three times the terrace's length, the origin of this spectral variation may originate from step-meandering. Indeed, in a step-flow growth mode, when adatoms reach the surface then can diffuse either towards the upper or lower step-edges. However, in general, the adatom capture probability at a step edge depends on the direction from which adsorbed atoms approach the step. Such asymmetry causes growth instability and can lead to the kinetic formation of such step-meandering.[20–22] This meandering induces a variation of the peak energy characterized by a standard deviation of 8 meV. Finally, it should be noted that no significant correlation between peak energy and CL intensity was found as illustrated in figure 3(c).

In contrast, the CL intensity map obtained for sample B and displayed in figure 3(d) reveals a clear correlation with threading dislocations. More precisely, the CL intensity exhibits local maxima in the vicinity of dislocations. This corresponds to a minimum in peak energy as shown in figure 3(e), suggesting that dislocation mediated spiral growth favours the incorporation of Ga in the vicinity of dislocations, as also observed by Funato *et al.*[23] As a consequence, the increased Ga concentration in this region tends to create efficient localization centers for electron-hole pairs from where they can efficiently recombine radiatively, spatially separated from point defects. This hypothesis is supported by the clear anti-correlation between CL intensity and peak energy shown in figure 3(f). We note here that similar findings, *i.e.* the influence of growth modes on IQE, were reported by Fuhrmann *et al.*[24] By employing growth conditions which benefit the formation of V-pits, they were able to enhance the

degree of carrier localization near dislocations, eventually improving the IQE of GaN/AlGaN QW structures.

To further confirm our interpretation of carrier recombination governed by localization effects, temperature-dependent time-resolved CL spectroscopy was performed.

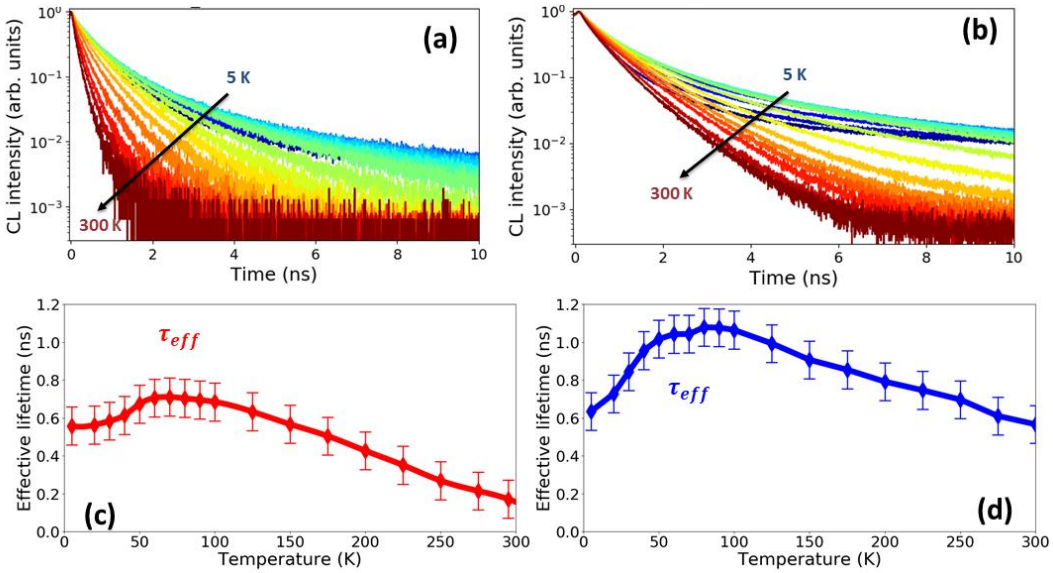

Fig. 4. (a, b) Normalized CL decay transients of the MQW emission at varying temperatures for sample A (a) and sample B (b). (c, d) Average carrier lifetime (τ_{eff}) with temperature for sample A (c) and sample B (d).

Figure 4(a) (figure 4(b)) displays the CL decay transients for sample A (sample B) for different temperatures ranging from 5 K up to room temperature. We note here that the CL decay cannot be modelled by a simple mono-exponential function regardless of temperature and sample. This further suggests that localization plays an important role in the carrier recombination dynamics.[25,26] To fully capture the complex recombination dynamics, the CL decay transients were fitted satisfactorily using the bi-exponential function $I_{CL}(t) = A_1\, exp\left(-\frac{t}{\tau_1}\right) + A_2 \exp\left(-\frac{t}{\tau_2}\right)$.[27] The weighted averages $\tau_{eff} = \frac{A_1\tau_1 + A_2\tau_2}{A_1 + A_2}$ of the carrier decay times are displayed in figure 4(c, d).

Both samples exhibit qualitatively similar trends, albeit deviating in certain important parameters. The carrier decay time of sample A is found to increase with temperature from 550 ps (T = 5K) up to 710 ps (T = 70K), followed by a pronounced decrease of decay time down to 200 ps at room temperature. Employing the model of carrier localization, this non-monotonic behaviour is explained as follows. At

low temperatures close to absolute zero, carriers are randomly distributed among available potential minima. When the temperature is increased, carrier mobility is enhanced, enabling them to hop into more deeply localized states. Simultaneously, carrier lifetime increases due to reduced wave function overlap of the electron-hole pairs. When the temperature increased further (T > 70 K), an increasing fraction of carriers becomes delocalized. Consequently, carrier lifetimes decrease again as carrier mobility is high enough for them to reach non-radiative recombination centers. In case of sample B we observe a similar trend, but with the carrier redistribution at low temperatures being more pronounced, with an increase of lifetimes from 630 ps at T = 5 K up to 1080 ps at T = 100 K. In addition, the activation of non-radiative recombination channels is less pronounced for sample B since the carrier lifetime only drops to 570 ps at room temperature.

Both the increased carrier lifetime at room temperature as well as the higher temperature for which the maximum of the carrier lifetime is reached indicates that there is a larger degree of carrier localization in sample B. As a consequence, carriers are – on average – distributed to more deeply localized states for elevated temperatures, which results in a more pronounced increase of the lifetime with temperature. Similarly, since the carriers in sample B are less mobile, the non-radiative recombination at point defects is reduced, directly improving the room temperature IQE.

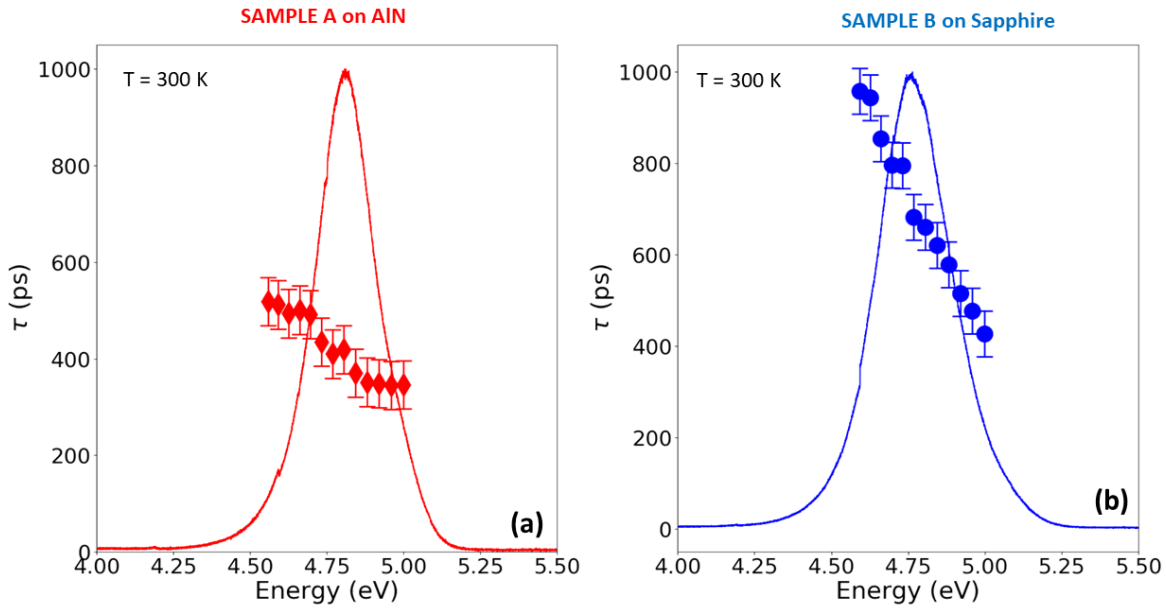

Fig. 5. Time-integrated CL spectrum and the emission lifetime as a function of photon energy at room temperature for sample A (a) and sample B (b).

Finally, to confirm the beneficial impact of carrier localization strength even at room temperature, the dependence of the CL decay time as a function of detection photon energy is shown in figure 5. According to Chichibu *et al.*, this evolution should be governed by the carrier localization energies.[28] If all carriers in the QW are in thermal equilibrium (*i.e.* not influenced by localization), the lifetime is expected to be independent of the photon energy. On the contrary, if the QW emission originates from the recombination of carriers independently localized among potential minima of varying depth, lifetimes are expected to be highly dependent on detection photon energy, with higher-energetic photons corresponding to shorter lifetimes (*i.e.* more weakly localized carriers). This behaviour is observed in both samples. However, in case of sample A, the lifetime only changes slightly from 500 ps at a detection energy of 4.5 eV down to 350 ps at 5 eV. In contrast, sample B reveals a significant decrease in carrier lifetime from 950 ps to 400 ps for the same energetic range. This observation can be regarded as clear evidence that carrier recombination is governed by localization even at room temperature for both samples, albeit a significantly greater impact of the effect is found in sample B, providing an explanation for the higher IQE.

IV. CONCLUSIONS

In conclusion, we studied the origin of the higher IQE measured in a deep UV MQW structure grown on sapphire compared to a nominally identical MQW structure grown on native AlN. We found that dislocation-mediated spiral growth in the MQW region on sapphire substrates generally leads to the more efficient localization of carriers, which in turn helps to prevents carriers to recombine non-radiatively on point defects. For this reason, we propose that the IQE of the active region of a DUV LED may be improved both by exploiting the carrier localization through specific choices of growth mode as well as reducing the point defect density itself. Nevertheless, both factors are crucial for DUV LED operation and need to be studied and understood in greater detail in order for such devices to close the gap to the already widely available, highly efficient products emitting in the visible spectral range.

Ackowledgments

G.J acknowledges the financial support of the French National Research Agency in the framework of the "Investissements d'avenir" program (ANR-15-IDEX-02).

Data availability

The data that support the findings of this study are available from the corresponding author upon reasonable request.

References

[1] M. Kneissl, *III-Nitride Ultraviolet Emitters* (Springer International Publishing, 2016).

[2] T. Takano, T. Mino, J. Sakai, N. Noguchi, K. Tsubaki, and H. Hirayama, Appl. Phys. Express **10**, 031002 (2017).

[3] S. Max, S. Wenhong, L. Alex, H. Xuhong, D. Alex, B. Yuri, Y. Jinwei, S. Michael, G. Remis, M. Craig, G. Gregory, and W. Michael, Appl. Phys. Express **5**, 82101 (2012).

[4] C. Frankerl, M.P. Hoffmann, F. Nippert, H. Wang, C. Brandl, N. Tillner, H.-J. Lugauer, R. Zeisel, A. Hoffmann, and M.J. Davies, J. Appl. Phys. **126**, 075703 (2019).

[5] R. Kirste, Q. Guo, J.H. Dycus, A. Franke, S. Mita, B. Sarkar, P. Reddy, J.M. LeBeau, R. Collazo, and Z. Sitar, Appl. Phys. Express **11**, 082101 (2018).

[6] F. Nippert, M. Tollabi Mazraehno, M.J. Davies, M.P. Hoffmann, H.-J. Lugauer, T. Kure, M. Kneissl, A. Hoffmann, and M.R. Wagner, Appl. Phys. Lett. **113**, 071107 (2018).

[7] J.P. Ibbetson, P.T. Fini, K.D. Ness, S.P. DenBaars, J.S. Speck, and U.K. Mishra, Appl. Phys. Lett. **77**, 250 (2000).

[8] F. Donatini and J. Pernot, Nanotechnology **29**, 105703 (2018).

[9] S. Meuret, M. Solà Garcia, T. Coenen, E. Kieft, H. Zeijlemaker, M. Lätzel, S. Christiansen, S.Y. Woo, Y.H. Ra, Z. Mi, and A. Polman, Ultramicroscopy **197**, 28 (2019).

[10] W. Liu, J.-F. Carlin, N. Grandjean, B. Deveaud, and G. Jacopin, Appl. Phys. Lett. **109**, 042101 (2016).

[11] T. Oto, R.G. Banal, K. Kataoka, M. Funato, and Y. Kawakami, Nat. Photonics **4**, 767 (2010).

[12] R.G. Banal, M. Funato, and Y. Kawakami, Appl. Phys. Lett. **99**, 011902 (2011).

[13] K. Ban, J. Yamamoto, K. Takeda, K. Ide, M. Iwaya, T. Takeuchi, S. Kamiyama, I. Akasaki, and H. Amano, Appl. Phys. Express **4**, 052101 (2011).

[14] B. Liu, R. Zhang, J.G. Zheng, X.L. Ji, D.Y. Fu, Z.L. Xie, D.J. Chen, P. Chen, R.L. Jiang, and Y.D. Zheng, Appl. Phys. Lett. **98**, 261916 (2011).

[15] G. Rossbach, M. Feneberg, M. Röppischer, C. Werner, N. Esser, C. Cobet, T. Meisch, K. Thonke, A. Dadgar, J. Bläsing, A. Krost, and R. Goldhahn, Phys. Rev. B **83**, 195202 (2011).

[16] B. Gil, editor , *III-Nitride Semiconductors and Their Modern Devices* (Oxford University Press, 2013).

[17] J. Houston Dycus, S. Washiyama, T.B. Eldred, Y. Guan, R. Kirste, S. Mita, Z. Sitar, R. Collazo, and J.M. LeBeau, Appl. Phys. Lett. **114**, 031602 (2019).

[18] C. Haller, J.-F. Carlin, G. Jacopin, D. Martin, R. Butté, and N. Grandjean, Appl. Phys. Lett. **111**, 262101 (2017).

[19] W.K. Burton, N. Cabrera, and F.C. Frank, Philos. Trans. R. Soc. A Math. Phys. Eng. Sci. **243**, 299 (1951).

[20] A. Mogilatenko, J. Enslin, A. Knauer, F. Mehnke, K. Bellmann, T. Wernicke, M. Weyers, and M. Kneissl, Semicond. Sci. Technol. **30**, 114010 (2015).

[21] N.A.K. Kaufmann, L. Lahourcade, B. Hourahine, D. Martin, and N. Grandjean, J. Cryst. Growth **433**, 36 (2016).

[22] T.K. Uždavinys, S. Marcinkevičius, M. Mensi, L. Lahourcade, J.-F. Carlin, D. Martin, R. Butté, and N. Grandjean, Appl. Phys. Express **11**, 051004 (2018).

[23] M. Funato, R.G. Banal, and Y. Kawakami, AIP Adv. **5**, 117115 (2015).

[24] D. Fuhrmann, T. Retzlaff, M. Greve, L. Hoffmann, H. Bremers, U. Rossow, A. Hangleiter, P.

Hinze, and G. Ade, Phys. Rev. B **79**, 073303 (2009).

[25] A. Morel, P. Lefebvre, S. Kalliakos, T. Taliercio, T. Bretagnon, and B. Gil, Phys. Rev. B **68**, 045331 (2003).

[26] C.-N. Brosseau, M. Perrin, C. Silva, and R. Leonelli, Phys. Rev. B **82**, 085305 (2010).

[27] P. Lefebvre, C. Brimont, P. Valvin, B. Gil, H. Miyake, and K. Hiramatsu, Phys. Status Solidi **211**, 765 (2014).

[28] S.F. Chichibu, T. Azuhata, H. Okumura, A. Tackeuchi, T. Sota, and T. Mukai, Appl. Surf. Sci. **190**, 330 (2002).